 CMES, vol.100, no.4, pp.277-294, 2014

Establishment and Stability Analysis of a Hybrid Viscoelastic Model Based on Meshless for Surgical Robot System

Yidong Bao[1,2] **and Dongmei Wu**[1,3]

Abstract: Aiming at the shortcomings of mass-spring model, this paper, on the basis of preliminary studies, established a new viscoelastic soft tissue model based on meshless structure. The model is consisted of a large quantity of filled spheres, with every three spheres being connected by a spring and a Kelvin structure, which can further enhance the real-time virtual simulation operability while ensure the viscoelasticity of basic model. The stress relaxation and creep equation of the model can be derived from formula derivation. Through setting different parameters to the filled spheres, this model, with certain universal property, can create a virtual liver, kidney and skin soft tissue. By utilizing force feedback devices to handle different virtual soft tissue thus to get virtual simulation experimental data, then compare them with the actual characteristics data of soft tissue in published literature, and experiments have shown that this model possesses good stress-strain, stress relaxation and creep properties. Finally, this paper compared mass-spring model for the stress-strain and cutting simulation experiments, which further confirmed the effectiveness and stability of the proposed model.

Keywords: Virtual model, Viscoelastic model, Surgical robot, Mass-spring model.

1 Introduction

Robot assisted surgery has become the frontier and new technique in the current medical field. Applying this new technique requires doctors to be provided with proficient ability of operating robotic surgical apparatus. In order to achieve this goal, the doctors need continuous practice. However, it is not only in high-risk but also in high-cost to practice on human body or animal. So there emerged a virtual

[1] State Key Laboratory of Robotics and System, Harbin Institute of Technology, Harbin 150080, P. R. China.
[2] School of Software, Pingdingshan University, Pingdingshan 467000, P.R. China.
[3] Corresponding author. Email: wudmhit@163.com

surgical practicing system to supersede real surgical practicing process, which can not only reduce the risk and cost of surgery, but also realize repetitive practicing. [Picinbono, Delingette and Ayache (2001)] proposed that whether virtual surgery practicing is effective was closely related to the establishment of virtual soft tissue model; meanwhile an effective virtual soft tissue model can improve the quality and efficiency of the practicing.

Currently a lot of scholars have conducted research on the establishment of soft tissue models in virtual surgery practicing system, in which the most common ones are mass-spring model and finite element model. A mass-spring model uses spring to connect multiple mass points, and simulates the changes of soft tissue through the elasticity between springs, such as [Mohammadi (2009); Leon, Eliuk and Gomez (2010)]. The advantage of mass spring model lies in its simple structure, although it can ensure real-time, the accuracy is not high enough. Even though some researchers added auxiliary spring on the basis of the general mass spring model, the accuracy is improved ineffective. Finite element model is kind of a numerical technique to obtain approximate solutions to boundary value problems of partial differential equations, such as [Eskandari and Salcudean (2008); Khelifi, Rahim and Ratni (2013)]. Using finite element techniques to build a model can ensure a high accuracy, but cannot promise real-time in the process of real-time operation.

Soft tissues generally exhibit creep, relaxation, viscoelasticity. [Bel-Brunon, Kehl and Martin (2014)] proposed the non-linear viscoelastic behavior of lung parenchyma. [Fancello and Vassoler (2013)]proposed a model for viscoelastic materials with fiber reinforcement. [Martin, Kutluay and Yazicioglu (2013)] presents a soft tissue model based on generalized-Maxwell-type material models.[Moreira, Liu and Zemiti (2012)] presents a force control scheme based on a viscoelastic interaction model.

The main drawback of these methods based on mesh theory is generation of ill-shaped elements that cause numerical instability in the simulation [Jung and Lee (2012)]. Recently, meshless methods applied in many areas. And researchers use the meshless method to set up the model, such as potential energy method [Ishii and Sugii (2012)], discrete mechanics [Guess, Liu and Bhashyam (2013)], smoothed particle hydrodynamics (SPH)[Tong and Browne (2014)]. [Tavares, Belinha and Dinis (2014)] proposed the strain, the stress distribution, and the fracture resistance of restored teeth based on meshless method.[Kumar and Drathi (2014)] present a meshless Crack Particles Approach for ductile material failure.

This paper, on the basis of analyzing the characteristics of real soft tissue real, built a kind of virtual soft tissue model with viscoelasticity based on meshless structure. By setting different parameters, the model is qualified with certain universal prop-

erty. Through comparison between virtual model simulations operating data and the properties of real soft tissue in the existing published literature to get effective viscoelastic properties, thus confirmed the validity of the virtual soft tissue model. The comparison of cutting and creep between the proposed model in this article and the mass-spring model has further validated the stability of this model.

2 Material and methods

2.1 Mass-spring model

A mass-spring model has n mass points, every two of which are respectively connected with a spring, wherein the spring possesses a linear elastic coefficient, and follows Hooke's theorem. The position of mass points are under the influence of the elastic force of the inside spring and the external force of objects. When multiple forces are imposed on a mass point, the joint force equals with the vector sum of these forces. For every node in this model, the total spring forces for one node can be defined:

$$F_{M_i} = \sum_{\Delta M_i \in S_i} E_j(||M_j - M_i|| - x_j^0) \frac{M_j - M_i}{||M_j - M_i||} \tag{1}$$

where E_j is the coefficient of spring of node j which connects with i. M_i and M_j are the three-dimensional of the i and j, x_j^0 is the original length of the spring which connects with j. S_i is the set of all nodes, which connects with i.

2.2 Layered filled sphere structure viscoelastic model

When the mass point spring structure is under force, due to acceleration problems, the viscoelasticity of the established soft tissue model is not obvious, even if add an auxiliary spring, there is not much difference. On this basis, this paper proposed a meshless viscoelastic structure. This viscoelastic structure that consists of Kelvin model and connected with a spring has viscoelastic properties like creep and stress relaxation. Fig. 1 shows the different kinds of model structures.

As shown in Fig. 1(c), K_1 and K_2 indicates the elastic modulus of spring, v_1 means viscous modulus, $\sigma(t)$ means the stress value, and $\varepsilon_1(t)$ and $\varepsilon_2(t)$ mean the elongation length of spring at t moment.

Soft tissue model in this paper is achieved through adoption the above viscoelastic structure, this model consists of spheres in the same radius sphere, of which spheres are connected with viscoelastic structures. The sphere radius is set depending on the different model structure, if the radius is too large, the accuracy will be reduced; if it is too small, the real-time is not longer guaranteed. The model structure is shown in Fig. 2. While setting the soft tissue model structure, the structure used

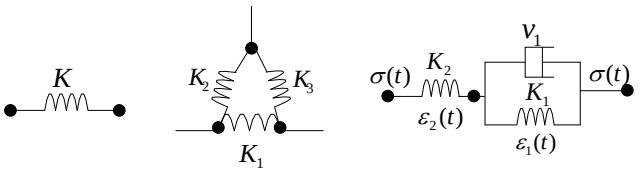

Figure 1: Three different structures for soft tissue model, (a) Mass-spring structure, (b) Added angle mass-spring structure, (c) CTPM structure.

in the beginning between the two spheres in the model is three-parameter nonlinear viscoelastic structure (TPM), but the subsequent experiments revealed that due to the complexity of the mathematical model, the calculation amount of the model is large, and its real-time is relatively poor. Therefore, on the basis of experimental verification, this paper proposed a three spheres structure shares a TPM structure. Model established in this way not only significantly reduced the amount of calculation, and represented a good real-time performance, but also the viscoelastic effective turned out to be quite well.

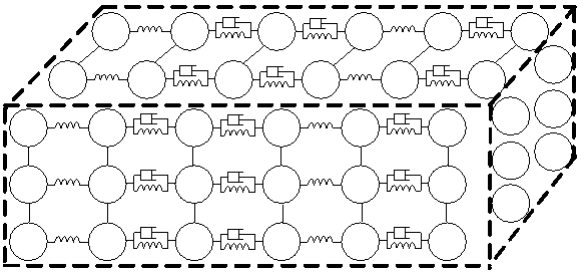

Figure 2: Layered filled sphere structure.

According to the data obtained from [Schwartz and Denninger (2005)] experiment, the tissue can be damaged once the strain is greater than 12*mm* when using a rigid ball to contact the liver soft tissue. Therefore, while proving the model proposed in this paper, the radius of the rigid ball of the contact model was set as 2*mm*, and the maximum strain was set as 12*mm*. Local force analysis of the model is shown in Fig. 3.

It is assume that at the outermost layer of the model there are five spheres, A_o, B_o, C_o, D_o, E_o respectively stands for the sphere center of phere A, B, C, D, E; A and B is connected with a spring, B and C is connected with Kelvin structure, D and E

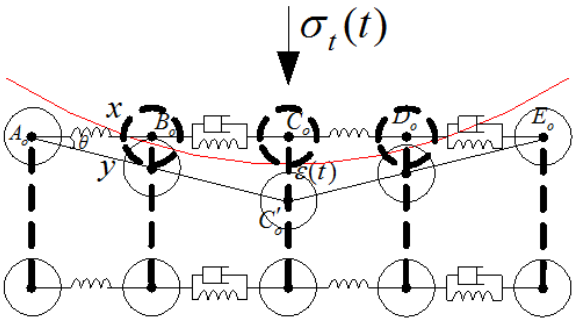

Figure 3: The stress status of CTPM under external force.

shares similar structure. Suppose the length between A_o and C_o is x, when sphere C is subjected to the action of force $F_x(x)$, the position of the sphere center C_o turns into C'_o, assume the length between A_o and C'_o is y, C_o and C'_o is $\varepsilon(t)$, the intersection angle between the x and y is θ. In order to reduce the amount of calculation, here suppose the displacement of A and E does not change. Besides the external force $\sigma_1(t)$ in the vertical plane and the vertical upright internal force $\sigma_2(t)$, sphere C is also subjected to the vertically upward component force $\sigma_c(t)$ between the A, C and E. And $\sigma_c(t)$ can be defined as:

$$\sigma_c(t) = 2E'\varepsilon(t)\left(\frac{1-\cos\theta}{\sin\theta}\right)\sin\theta \tag{2}$$

where, E' is the elastic modular. This assume that $\lambda = 2E'(1-\cos\theta)$.

2.3 Simulation condition

The experimental platforms in this paper are that include a force-feedback devices Omega.7 and a laptop which consist of Intel 2.3GHz CPU 4.0GB RAM. The simulation programs of virtual environment setting and force-feedback effect come from the Swiss Force Dimension Company (http://www.chai3d.org /download.html).

3 Model equation

Via improvements and experimental validation on the early models, in order to satisfy the effective value of strain under relatively big strained conditions, constraints were introduced on the basis of TPM. So this paper established the viscoelastic soft tissue model based on constraint three-parameter nonlinear viscoelastic structure (CTPM).

The formula of this model includes:

$$\sigma_o(t) = K_1\varepsilon_1(t) + v_1\dot{\varepsilon}_1(t) \tag{3}$$

$$\sigma_o(t) = K_2\varepsilon_2(t), \tag{4}$$

$$\sigma_c(t) = \lambda \cdot \varepsilon(t), \tag{5}$$

$$\varepsilon(t) = \varepsilon_1(t) + \varepsilon_2(t) \tag{6}$$

$$\sigma_t(t) = \sigma_o(t) + \sigma_c(t) \tag{7}$$

$$\sigma(t) = \frac{\sigma_t(t)}{1+\tan\theta} \tag{8}$$

By using Laplace transform and inverse Laplace transform, the formula of this model can be written as

$$\begin{aligned} &K_1K_2\varepsilon(t) + K_2v_1\dot{\varepsilon}(t) + \lambda(K_1+K_2)\varepsilon(t) + \lambda v_1\dot{\varepsilon}(t) \\ &= [(K_1+K_2)\sigma(t) + v_1\dot{\sigma}(t)](1+\tan\theta) \end{aligned} \tag{9}$$

This assumes that $P_1 = \frac{v_1}{K_1+K_2}$, $P_2 = \frac{K_1K_2}{K_1+K_2}$, $P_3 = \frac{v_1K_2}{K_1+K_2}$, Eq. 9 can be written as

$$(P_2+\lambda)\varepsilon(t) + (P_3+\lambda P_1)\dot{\varepsilon}(t) = [\sigma(t) + P_1\dot{\sigma}(t)](1+\tan\theta) \tag{10}$$

Eq. 10 is the constitutive equations of CTPM.

After noting that $x(t) = x_0H(t)$, the relaxation equations of CTPM can be written as

$$\sigma(t) = \frac{(K_2+\lambda)\varepsilon_0 - \frac{K_2^2\varepsilon_0}{K_1+K_2}(1-e^{-t(K_1+K_2)/v_1})}{1+\tan\theta} \tag{11}$$

Similarly, the creep equations of CTPM can be written as

$$\varepsilon(t) = \frac{\sigma_0(1+\tan\theta)}{P_3+\lambda P_1}\left[\frac{P_3+\lambda P_1}{P_2+\lambda}(1-e^{-t\frac{P_2+\lambda}{P_3+\lambda P_1}}) + P_1e^{-t\frac{P_2+\lambda}{P_3+\lambda P_1}}\right] \tag{12}$$

And noting that when $t = 0^+$, Eq. 11 can be written as

$$\sigma(0^+) = \frac{(K_2+\lambda)\varepsilon_0}{1+\tan\theta} \tag{13}$$

Similarly, when $t \to \infty$, Eq. 11 can be written as

$$\sigma(\infty) = \frac{(K_2+\lambda)\varepsilon_0 - \frac{K_2^2\varepsilon_0}{K_1+K_2}}{1+\tan\theta} \tag{14}$$

Noting that when $t = 0^+$, Eq. 12 can be written as

$$\varepsilon(0^+) = \frac{\sigma_0(1+\tan\theta)}{\lambda + K_2} \tag{15}$$

Similarly, noting that when $t \to \infty$, Eq. 12 can be written as

$$\varepsilon(\infty) = \frac{\sigma_0(1+\tan\theta)}{\lambda + K_2} + \frac{(K_1+K_2)\sigma_0(1+\tan\theta)}{\lambda(K_1+K_2)+K_1K_2} \tag{16}$$

4 Model parameters

[Carter, Frank and Davies (2001)] inserted hand-held detection device into the abdomen, and measured the elastic model of pig liver was about $490Kpa$, and that of human liver was about $270Kpa$. [Ottensmeyer and Salisbury (2000)] exploited assist robot and sophisticated sensors equipment and measured the liver elastic model to be $10-15Kpa$. The elastic modulus obtained through the second method is more accurate. On meet the theoretical principles of [Lee and Radok (1959)], this paper utilized rigid balls of small radius to verify the validity of this model. The median stress at the probing point is given by

$$\sigma = \frac{F}{S_0} \tag{17}$$

where, S_0 is the probe area.

For different soft tissue organs, set different elastic modulus parameters to satisfy their different stress-strain characteristics. The elastic modulus parameter range for different soft tissue models in this paper was 10-14Kpa.

The soft tissue viscous modulus [Klatt, Hamhaber and Asbach (2007)] obtained using the Z model experiment was about 5.5 ± 1.6 $Pa.s$. Through simulation of human liver characteristics, the viscous modulus [Asbach, Klatt and Hamhaber (2008)] got from experiment was about $5Pa.s$. According to different soft tissue models, this paper selected the viscous modulus parameter range to be 0.8-7 $Pa.s$.

5 Results and discussion

5.1 Analysis of stress-strain for different virtual model

[Belkoff and Haut (1991)] carried out experiments on one month-old mice to detect data concerning about the stress-strain of skin. [Al-ja'afreh, Zweiri and Seneviratne (2008)] applied a radius of 1mm rigid ball to contact kidneys so as to detect the stress-strain data of kidney. [Evren, Mert and Cagatay (2007)] inserted a rigid probe into the abdominal cavity to detect liver stress-strain and stress relaxation

data. Furthermore, [Amy, Mark and Robert (2006)] detected the liver creep data by load different stress on the liver. Through the virtual model simulation to prove the effectiveness and consistency of the virtual model established in this paper with data those experiments above testified, including the stress-strain data of skin and kidney and the stress-strain, stress relaxation and creep data of liver. Fig. 4 shows the different virtual soft models based on CTPM by VC++ and OpenGL.

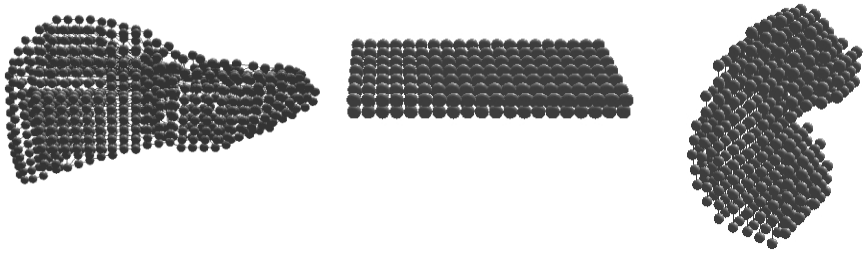

(a) (b) (c)

Figure 4: (a) Virtual liver model (b) Virtual skin model (c) Virtual kidney model.

5.1.1 Stress-strain of virtual skin model

According to the skin of stress-strain values that [Belkoff and Haut (1991)] obtained through experiments, in the virtual skin model established in this paper, the radius of the sphere was set as $7mm$, and the length between each of the two spheres was $7mm$. In accordance with Eq. 11 and Eq. 12, the parameter $K_1 = 82kPa$, $K_2 = 82kPa$, $K' = 164kPa$, $v_1 = 3Pa \cdot s$ are chosen in skin model. Among the force components of the model, parameter λ changes with the strain, different strain produce different λ values, as shown in Table 1. By using a $2.8mm$ rigid ball to contact virtual skin model, and compared the result with the real skin stress-strain data in the [Belkoff and Haut (1991)]. In addition, the paper further validated the effectiveness of the later on improved model by comparing the results of preliminary studies. In early models, the stress increases with the strain, but when the strain exceeds $8mm$, the stress goes beyond the actual stress value. To overcome this defect in this paper, on the basis of preliminary studies, added a constraint parameter to the stress, which decreases with the increasing of the strain so as to make sure that the stress is within the real experimental data range. The comparison result is shown in Fig. 5. As can be seen from the figure, the model with constraints are more stable than the previous models, meanwhile the stress-strain data of virtual skin model is identical with that of real skin, which has confirmed the validity of the virtual skin model.

Table 1: The value of λ_s, λ_k, λ_l and comparison among the strain of TPM and CTPM for different soft tissues.

x (mm)	Skin			Kidney			Liver		
	λ_s (kPa)	$F_{is}(t)$ (TPM)	$F_s(t)$ (CTPM)	λ_k (kPa)	$F_{ik}(t)$ (TPM)	$F_k(t)$ (CTPM)	λ_l (kPa)	$F_{il}(t)$ (TPM)	$F_l(t)$ (CTPM)
2	0.37	1.6	1.7	0.73	0.42	0.37	0.14	0.19	0.17
4	1.47	3.9	3.6	2.9	0.8	0.7	0.54	0.4	0.25
6	3.3	6.1	5.7	6.3	1.5	1.2	1.2	0.66	0.38
8	5.8	9.2	7.7	10.8	2.2	1.7	2.1	0.96	0.62
10	8.9	12.3	9.9	16.3	3.2	2.3	3.1	1.3	0.84
12	12.6	15.8	12.3	22.4	4.5	3.0	4.2	1.8	1.1

5.1.2 Stress-strain of virtual kidney model

According to the kidney of stress-strain values that [Al-ja'afreh, Zweiri and Seneviratne (2008)] obtained through experiments, in the virtual kidney model established in this paper, the radius of the sphere was set as $4mm$, and the length between each of the two spheres was $4mm$. In accordance with Eq. 11 and Eq. 12, the parameter $K_1 = 58kPa$, $K_2 = 58kPa$, $K' = 106kPa$, $v_1 = 4Pa \cdot s$ are chosen in kidney model. By using a $1.5mm$ rigid ball to contact virtual kidney model, and compared the result with the real kidney stress-strain data in the [Al-ja'afreh, Zweiri and Seneviratne (2008)]. The comparison result is shown in Fig. 5. As can be seen from the figure, the model with constraints are more stable than the previous models, meanwhile the stress-strain data of virtual kidney model is identical with that of real kidney, which has confirmed the validity of the virtual kidney model.

5.1.3 Stress-strain and relaxation of virtual liver model

According to the liver of stress-strain values that [Evren, Mert and Cagatay (2007)] obtained through experiments, in the virtual liver model established in this paper, the radius of the sphere was set as $4mm$, and the length between each of the two spheres was $4mm$. In accordance with Eq. 11 and Eq. 12, the parameter $K_1 = 15kPa$, $K_2 = 15kPa$, $K' = 20kPa$, $v_1 = 5Pa \cdot s$ are chosen in liver model. By using a $2mm$ rigid ball to contact virtual liver model, and compared the result with the real liver stress-strain data in the [Evren, Mert and Cagatay (2007)]. The comparison result is shown in Fig. 6. Moreover, [Evren, Mert and Cagatay (2007)] utilizing monitoring facilities to conduct experiments and obtained that the liver stress relaxation in 30 seconds was 4 mm. The comparison between the simulation

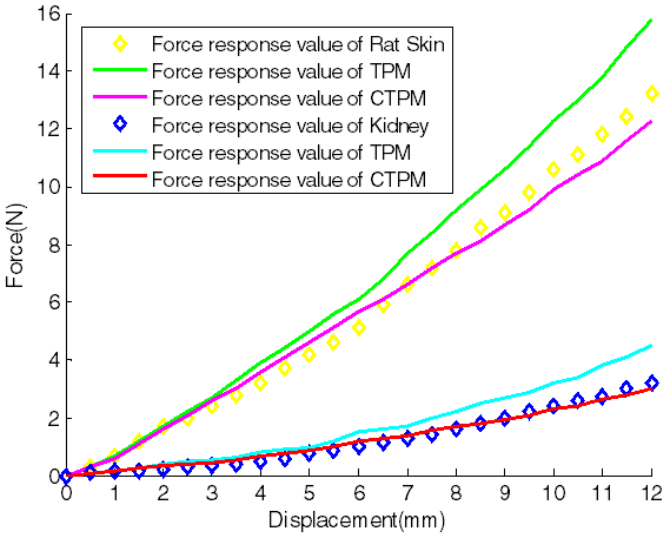

Figure 5: Comparison among the force response of TPM , CTPM and the real soft tissue experimental data of Skin, Kidney.

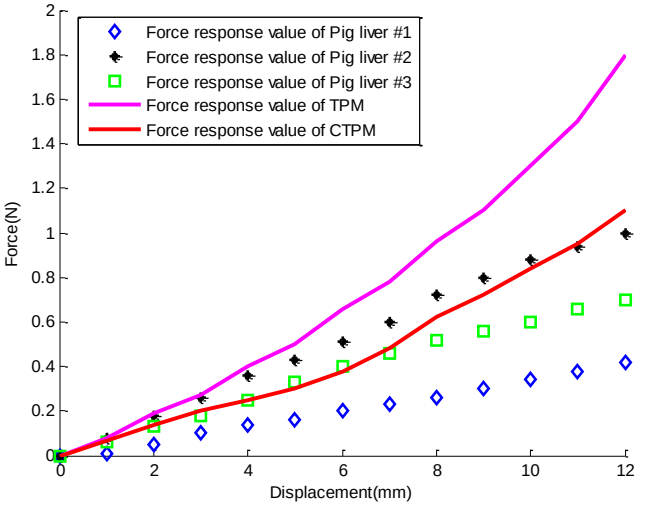

Figure 6: Comparison among the force response of TPM , CTPM and the real soft tissue experimental data of three pig livers.

data of relaxation of liver and the experimental data obtained by [Evren, Mert and Cagatay (2007)] is shown in Fig. 7. As can be seen from the Fig. 6 and Fig. 7, the model with constraints are more stable than the previous models, meanwhile the stress-strain and relaxation data of virtual liver model is identical with that of real liver, which has confirmed the validity of the virtual liver model.

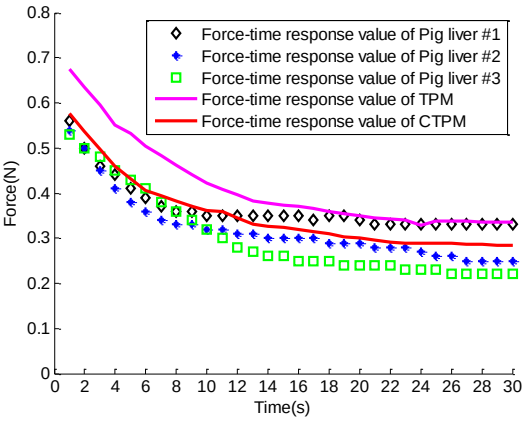

Figure 7: Comparison among the stress relaxation experiment data of real soft tissue, simulation data of unconstrained model and constrained model in 3 seconds with a speed of $2mm/s$ and a strain of $4mm$.

5.1.4 Creep of virtual liver model

Moreover, [Amy, Mark and Robert (2006)] monitored the strain range of a liver subjected to a $0.98N$and $0.196N$ force in 33 seconds was 3.8-6.65 mm and 9.6-11.9mmthrough the experiment. The comparison between the simulation data of creep of liver and the experimental data obtained by [Amy, Mark and Robert (2006)] is shown in Fig. 8. As can be seen from the Fig. 8, the model with constraints are more stable than the previous models, meanwhile the creep data of virtual liver model is identical with that of real liver, which has confirmed the validity of the virtual liver model.

5.2 Analysis of stress-strain for mass-spring model and CTPM

Fig. 9 shows the model surface and internal changes of the different structural forms between spheres in the model when imposed with forces. In Fig. 9(a) the structure that connected the two spheres is mass-spring structure; and in Fig. 9(b) it is a CTPM structure. From the performance of these different structures applying

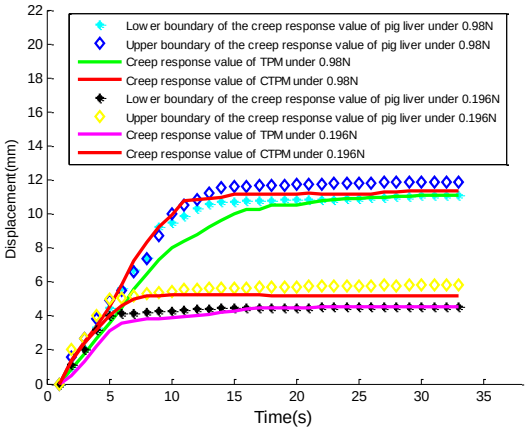

Figure 8: Comparison among the creep experiment data of real soft tissue, simulation data of unconstrained model and constrained model when load $0.98N$ and $0.196N$ forces onto the liver soft tissue in the vertical Z-axis direction.

with forces, the mass-spring model shocked obviously, while the CTPM presented creep property, which was in line with the real soft tissue characteristics.

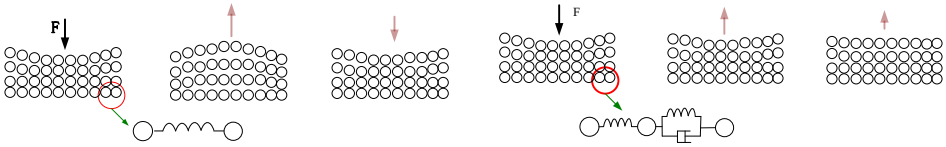

Figure 9: (a) The performance of mass-spring model applying with forces (b) T The performance of CTPM applying with forces.

Fig. 10 stands for the virtual liver soft tissue model using VC ++ programming, and in Fig. 10(a) the two spheres in the model is connected through a mass-spring structure; in Fig. 10(b) they are connected by a CTPM. Using a rigid ball to contact soft tissue model can prove that the contact position in Fig. 10(a) is rough, but that in Fig. 10(b) is smooth, which fits the after-contact characteristic of soft tissue.

To verify the validity of the CTPM, experiments were conducted to the mass-spring syntactic model and the CTPM to compare the stability of these models. A force of 0.13 N that perpendicular to the axis Z, at a speed of $4mm/s$, acted on sphere C and generated the creep effect drawing of the above-mentioned two different structures. Fig. 13 shows the distribution of a sphere under the action of force F. It can be

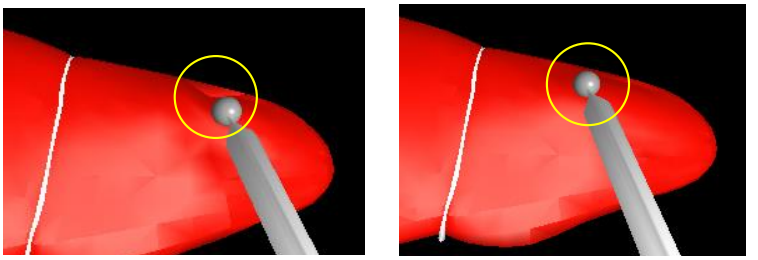

(a) (b)

Figure 10: Various effects of applying rigid balls to contact surfaces of the soft tissue model from the vertical Z-axis direction.

seen from the Fig.11, the mass-spring model has very obvious fluctuates, but the CTPM has obvious advantage in model structure and deformation.

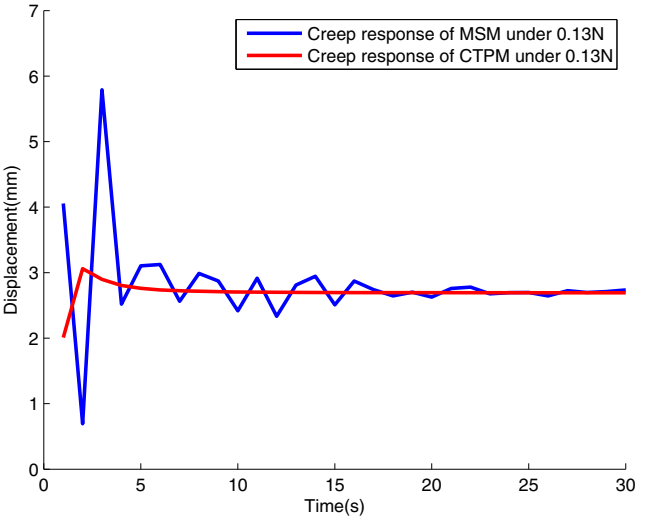

Figure 11: Comparison among the creep response of the mass-spring model and CTPM under $0.13N$ with the axis Z, at a speed of $4mm/s$.

5.3 Analysis of cutting simulation for mass-spring model and CTPM

To further verify the effectiveness of the CTPM, the cutting simulation experiments of the mass-spring model and the CTPM were included. Fig. 12 shows the cutting schematic view of the two different structures: after the cut, the cutting position of

the mass-spring structure model remained oscillating back and forth due to the elasticity, while the cutting position of the CTPM remained relative stable because of the influence of gravity and creep characteristic, which coincident with the cutting effect of real soft tissue.

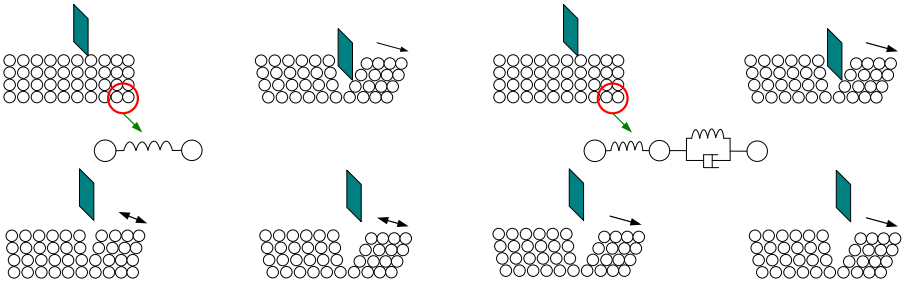

Figure 12: (a) The cutting simulation experiments of the mass-spring model (b) The cutting simulation experiments of the CTPM.

Through the cutting experiments of virtual kidney model to verify the stability of the same cutting positions in the mass-spring model and the CTPM. Point *A*, *B*, *C*, *D* in Fig. 13(b) corresponds to the red point *A*, *B*, *C*, *D* in the three-dimensional coordinates of Fig. 13(b). After the virtual cutting, the two sides of the cutting position were divided; different cutting effects were generated depending on the structural models.

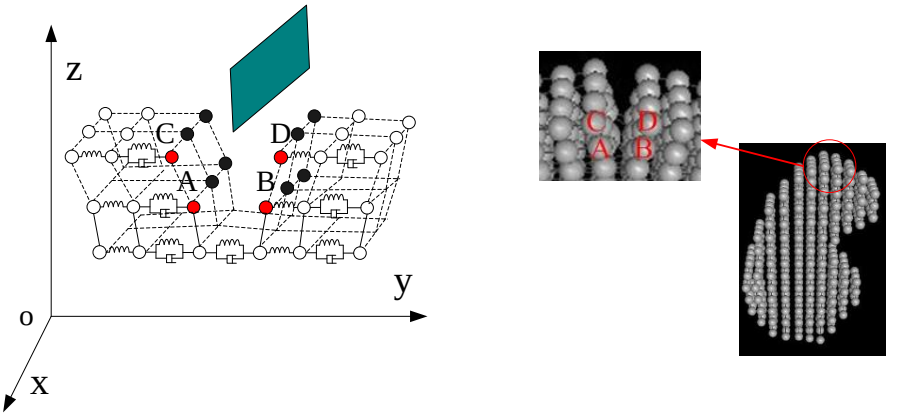

Figure 13: (a) The performance of cutting in three-dimensional coordinate, (b) The performance of cutting experimental in CTPM.

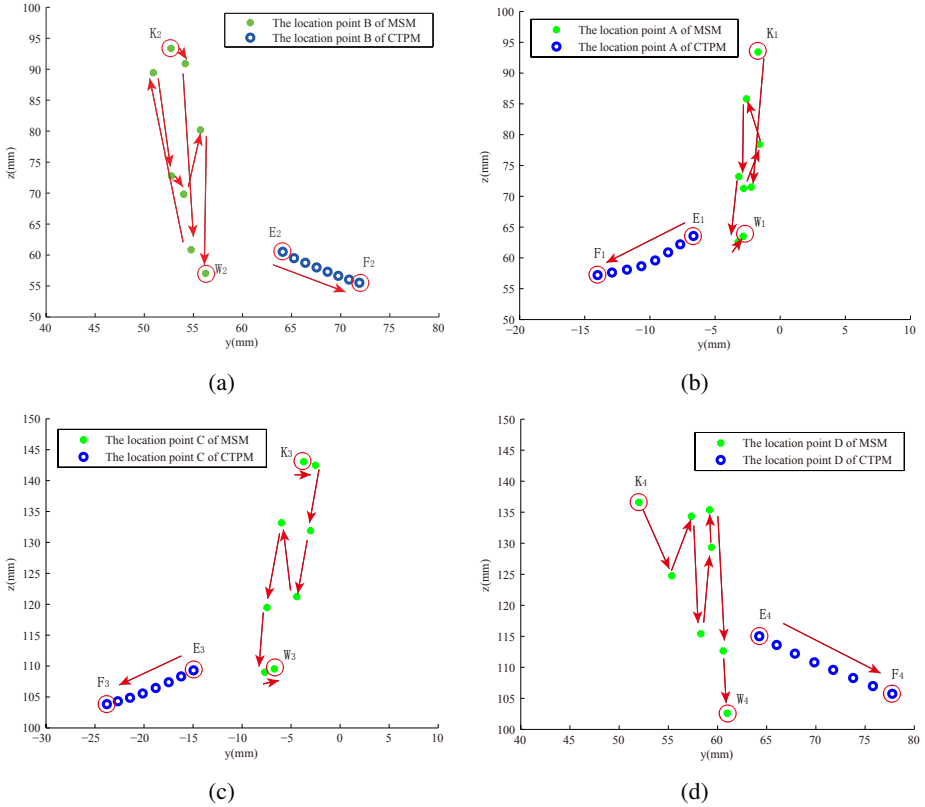

Figure 14: Comparison distribution of 8 coordinate values of (a) B, (b) A, (c) C, (d) D points in the model between which is connected by mass-spring and CTPM respectively between 1s and 8s.

In the three-dimensional coordinates of Fig. 13(a), the position each corresponding cut point in X-axis remained unchanged. The changes were reflected in the two-dimensional coordinates of the Y-axis and Z-axis. Fig. 14 represents the coordinate position change value of point A in the two-dimensional coordinates of the Y-axis and Z-axis obtained in every 1 second after the cut. Among which the blue point and cyan point respectively represent the coordinate position change value of point A changes with time in the CTPM and the mass-spring model; as shown in Fig. 14(b), where E_1 stands for the coordinate of A with 1 second after the cut in the CTPM, F_1 represents the coordinate value of point A with 8 seconds after the cut; K_1 represents the coordinate of point A with 1 second after the cut in the mass spring model, W_1 represents the coordinate 8 seconds after the cut, and the arrows indicates the coordinate position change in every 1 second. As can be seen from the

figure, after the cutting in the mass spring structure model, various points oscillate back and forth, and the points are of irregular distribution; while after the cutting in the three parameters model, points on both sides separate naturally, which is in line with the cutting effect of real soft tissue. Similarly, Fig. 14(a), Fig. 14(c), Fig. 14(d) show location changes of sphere A, C, D respectively.

6 Conclusion

By setting different parameters to the spring and Kelvin structure within the spheres, this model can represent different soft tissue structures. As to meshless structural filled spheres, the layer and number of filled spheres in soft tissue models can be set differently, the more levels and the larger number of filled spheres, the more accurate the model is, but the real-time performance becomes poor. While utilizing force feedback devices to operate virtual soft tissue model, the radius of rigid balls can affect the strain values of different soft tissues. In addition, the accuracy of virtual soft tissue model needs to be further improved, and the parameters setting for different soft tissues requires further test and verify to some extent. The follow-up work is to increase the layer and number of filled spheres in soft tissues and further improve the accuracy of the model on the premise of ensuring the system real-time; and launch related research about after-cut force analysis and cutting edge.

Acknowledgement: This work was supported by “the National Science Foundation of China” (NO. 61273358/F0306); and supported by "the Fundamental Research Funds for the Central Universities" (Grand No.HIT.IBRSEM.201320); and supported by “Self-Planned Taskof State Key Laboratory of Robotics and System(HIT)” (No. SKLRS2014013B).

References

Al-ja’afreh, T.; Zweiri, Y.; Seneviratne, L.; and Althoefer, K. (2008): A new soft-tissue indentation model for estimating circular indenter ‘force–displacement’ characteristics. *Engineering in Medicine*. vol. 222, pp. 805-815.

Amy, E. K.; Mark, P. O.; Robert, D. H. (2006): Effects of perfusion on the viscoelastic characteristics of liver. *Journal of Biomechanics*, vol.39, pp. 2221-2231.

Asbach, P.; Klatt, D.; Hamhaber, U.; Bram, U.; Somasundaram, R.; Hannn, B.; Sack, I. (2008): Assessment of Liver Viscoelasticity Using Multifrequency MR Elastogaphy. *Magpetic ReiDnance in Medicine*, vol.60, pp. 373-379.

Bel-Brunon, A.; Kehl, S.; Martin, C.; Uhlig, S.; Wall, W.A. (2014): Numerical identification method for the non-linear viscoelastic compressible behavior of soft

tissue using uniaxial tensile tests and image registration - Application to rat lung parenchyma. *Journal of the Mechanical Behavior of Biomedical Materials*, vol. 29, pp. 360-374.

Belkoff, S. M.; Haut, R. C. (1991): A structural model used to evaluate the changing microstructure of maturing rat skin. *Journal of Biomechanics*, vol. 24, no. 8, pp. 711-720.

Carter, F. J.; Frank, T. G.; Davies, P. J.; McLean, D.; Cuschieri, A. (2001): Measurement and modelling of the compliance of human andporcine organs. *Medical Image Analysis*, vol. 5, no. 4, pp. 231–236.

Eskandari, H.; Salcudean, S. E. (2008): Characterization of the viscosity and elasticity in soft tissue using dynamic finite elements. *Proc. IEEE Engineering in Medicine and Biology Society*, pp. 5573-5576.

Evren, S.; Mert, S.; Cagatay, B.; Levent, A.; Oktay, D. (2007): A robotic indenter for minimally invasive measurement and characterization of soft tissue response. *Medical Image Analysis*, vol. 11, pp. 361-373.

Fancello, E. A.; Vassoler, J. M. (2013): Variational viscoelastic-damage model for fiber reinforced soft tissues. *ASME 2013 Summer Bioengineering Conference*, vol. 1B.

Guess, T. M.; Liu, H.; Bhashyam, S.; Thiagarajan, G. (2013): A multibody knee model with discrete cartilage prediction of tibio-femoral contact mechanics. *Computer Methods in Biomechanics and Biomedical Engineering*, vol. 16, no. 3, pp. 256-270.

Ishii, E.; Sugii, T. (2012): Surface tension model for particle method using interparticle force derived from potential energy. *American Society of Mechanical Engineers, Fluids Engineering Division (Publication) FEDSM*, vol. 1, pp. 569-578.

Jung, H.; Lee, D. Y. (2012): Real-time cutting simulation of meshless deformable object using dynamic bounding volume hierarchy. *Computer animation and virtual worlds*, vol. 23, pp. 489-501.

Khelifi, R.; Rahim, M.; Ratni, B.; Rabehi, A.; Bellemare, M.-E. (2013): Simulation and evaluation of the strain of female pelvic organs with mass-spring and finite-elements models. *The International Society for Optical Engineering*, vol. 8922, pp. 12-18.

Klatt, D.; Hamhaber, U.; Asbach, P. (2007): Noninvasive assessment of the rheological behavior of human organs using multifrequency MR elastography: A study of brain and liver viscoelasticity. *Physics in Medicine and Biology*, vol. 52, no. 24, pp. 7281-7294.

Kumar, V.; Drathi, R. (2014). A meshless Cracking Particles Approach for ductile

fracture. *KSCE Journal of Civil Engineering*, vol. 18, no. 1, pp. 238-248.

Lee, E. H.; Radok, J. (1960) The contact problem for viscoelastic bodies. *Journal of Applied Mechanics,* vol. 27, no. 3, pp. 438-444.

Leon, C. A. D.; Eliuk, S.; Gomez, H. T. (2010): Simulating Soft Tissues Using a GPU Approach of the Mass-Spring Model. *Proc. IEEE Virtual Reality Conference (VR)*, pp. 261-262.

Martin, B. A.; Kutluay, U.; Yazicioglu, Y. (2013): Method for dynamic material property characterization of soft-tissue-mimicking isotropic viscoelastic materials using fractional damping models. *Journal of Testing and Evaluation*, vol. 41, no. 5.

Mohammadi, H. (2009): A numerical method to enhance the accuracy of mass-spring systems for modeling soft tissue deformations. *Journal of Applied Biomechanics*, vol. 25, no. 3, pp. 271-278.

Moreira, P.; Liu, C.; Zemiti, N.; Poignet, P.(2012): Soft tissue force control using active observers and viscoelastic interaction model. *Proc.IEEE International Conference on Robotics and Automation*, pp. 4660-4666.

Nealen, A.; Müller, M.; Keiser, R. (2006): Physically based deformable models in computer graphics. *Comput. Graph.Forum*, vol. 25, no. 4, pp. 809-836.

Ottensmeyer, M. P.; Salisbury, J. K. (2000): In vivo mechanical tissue property measurement for improved simulations. *Digitization of the Battlespace and Battlefield Biomedical Technologies*, vol. 4037, pp. 286-293.

Picinbono, G.; Delingette, H.; Ayache, N. (2001): Non-linear and anisotropic elastic soft tissue models for medical simulation. *Proc. IEEE International Conference Robotics and Automation*, vol. 2, pp. 1370-1375.

Schwartz, J. M.; Denninger, M.; Rancourt, D.; Moisan, C.; Laurendeau, D. (2005): Modelling liver tissue properties using a non-linear visco-elastic model for surgery simulation. *Medical Image Analysis*, vol. 9, pp. 103-112.

Tavares, C. S. S.; Belinha, J.; Dinis, L. M. J. S.; NatalJorge, R. M. (2014): Numerical analysis of a teeth restoration: A meshless method approach. *Proc. The 3rd International Conference on Biodental Engineering*, pp. 207-211.

Tong, M.; Browne, D. J. (2014): An incompressible multi-phase smoothed particle hydrodynamics (SPH) method for modelling thermocapillary flow. *International Journal of Heat and Mass Transfer*, vol. 73, pp. 284-292.